Electrostatic modes as a diagnostic in Penning-trap experiments

Carl S. Weimer, J. J. Bollinger, F. L. Moore,* and D. J. Wineland
Time and Frequency Division, National Institute of Standards & Technology, 325 Broadway, Boulder, Colorado 80303
(Received 4 October 1993)

A subset of the electrostatic modes of a cold cloud of electrons, a non-neutral electron plasma, trapped in a Penning trap has been observed and identified using a recent theoretical model. The detection of these modes is accomplished using electronic techniques which could apply to any ion species. The modes are observed in the low-density, low-rotation limit of the cloud where the cloud approaches a two-dimensional charged disk. We observe both axially symmetric and asymmetric drumhead modes. The shape, rotation frequency, and density of the cloud are found in a real-time nondestructive manner by measuring the frequency of these modes. In addition, it is found that radio-frequency sideband cooling compresses the cloud, increasing its density. The ability to measure and control the density of a trapped ion cloud might be useful for experiments on low-temperature ion–neutral-atom collisions, recombination rates, and studies of the confinement properties of non-neutral plasmas.

PACS number(s): 32.80.Pj, 35.80.+s, 52.25.Wz, 52.35.Fp

Penning ion traps have become an important tool in studies involving low-energy charged particles [1]. Recently, a theory of the electrostatic fluid modes of a plasma confined in a Penning trap (and Paul rf trap) was developed [2–4]. A number of these modes were observed experimentally in a plasma of Be^+ ions using optical fluorescence techniques [3,4]. By measuring the eigenfrequencies of two or more of these modes, plasma characteristics such as density, rotation frequency, and shape can be found nondestructively. Several types of experiment would benefit from this information. For example [1,4], experiments on recombination rates, ion–neutral-atom and ion-ion collisions, and strongly coupled systems depend on the ion sample density, size, and shape. These modes can also be used to study the confinement properties of the trap. However, a general method for detecting these modes is desired. Optical detection of the modes, as demonstrated in Ref. [3], is practical only for a small number of ion species. The method of characterizing the plasma by ejecting the plasma from the trap onto a set of charge collectors [5] has the disadvantage (for some experiments) of being a destructive measurement.

The object of the work reported here was to investigate detection techniques which would allow these mode frequencies to be measured nondestructively for any type of ion species. To do this, we used electronic methods for detecting the modes and electron plasmas to test the methods. Related observations with trapped ions have been made by Barlow, Jeffries, and Dunn [6], and with electrons and positrons by Tinkle, Greaves, and Surko [7]. In the low-density, low-rotation limit of the electron plasmas we were able to detect a number of modes. By comparing the frequency dependence of the detected modes with the theoretical model by Dubin [2,4], an identification of the modes was made. This allowed us to calculate the density and aspect ratio of the electron plasmas and study their evolution. By combining this information with a measurement of the number of electrons, the plasma size could then be determined.

A second goal of this work was to find a way to manipulate and increase the plasma density. For trapped atomic ions, lasers can be used to apply a torque to the plasma, compressing it and increasing its density [3,4,8]. In addition, lasers can be used to cool the atomic ion plasma, reducing its temperature to below 10 mK [8]. The possibility of compression of a non-neutral plasma by wave excitation has also been discussed [9]. In the work reported here, we found that the parametric coupling technique called magnetron sideband cooling [10,11] increased the electron plamsa density. This technique uses only radio-frequency fields, is independent of the internal structure of the ion, and therefore can be used for any type of ion. The ability to increase a trapped plasma's density and decrease its temperature is important for a number of experiments including proposals to produce antihydrogen [12]. A prominent candidate for antihydrogen formation is a three-body collision $(e^+,e^+,\bar{p})$ whose cross section scales as $n_0^2 T^{-9/2}$, where n_0 is the density and T the temperature [12,13].

*Present address: Dept. of Physics, University of Texas, Austin, TX 78712.

I. THEORY

A Penning trap [1,5,10,11] confines charged particles by combining static magnetic and electric fields. Referring to Fig. 1, a static voltage V_0 applied between the endcaps and ring forms a potential (in spherical coordinates),

$$\Phi(r,\theta,\phi)=V_0\sum_{n=0}^{\infty}c_{2n}(r/d)^{2n}P_{2n}(\cos\theta)\ , \tag{1}$$

where P_{2n} are the Legendre polynomials and c_{2n} are constants. Here $d=r_t/\sqrt{2}$ is a characteristic trap size, with r_t the ring's internal radius (for our trap, $d=3.54$ mm). The electrode shapes are designed so that the dominant term in the electrostatic expansion is that labeled by c_2. This results in a potential $V_0c_2[z^2-(x^2+y^2)/2]/2d^2$ which confines the electrons axially in a harmonic well. In this case, the axial center-of-mass (c.m.) motion of the electrons is the same as that of a single electron and has a frequency $\omega_z=(2c_2qV_0/md^2)^{1/2}$ where q/m is the charge-to-mass ratio. A homogeneous axial magnetic field B_0 is superimposed on this electric potential ensuring radial confinement. In the radial plane the center-of-mass motion is composed of two superimposed circular motions: the $\mathbf{E}\times\mathbf{B}$ (or magnetron) motion at frequency ω_m, and the modified cyclotron motion at frequency $\omega_c'=\omega_c-\omega_m$, where $\omega_c=qB_0/m$ (SI units). In general, $\frac{1}{2}\omega_z^2=\omega_m\omega_c'$, and for our experiments, $\omega_m\ll\omega_z\ll\omega_c'$.

Cryogenic cooling used in this work was capable of reducing the electron temperature to close to 4 K. For the magnetic fields used here, and with 4 K temperatures, the cyclotron radius of an electron was small compared with the distance of closest approach between two electrons. Under this condition the plasma is strongly magnetized and the coupling between motion parallel and perpendicular to the magnetic field is weak [14,15]. This may have resulted in two different temperatures for motion parallel and perpendicular to the magnetic field. Except for a possible difference in these temperatures, we assume the electrons had sufficient time to evolve (due to electron/electron collisions) to a state of thermal equilibrium. In an experiment [16] with electrons with eV energies, global equilibration times were measured to be about 1 s at $B_0=0.01$ T. This time should increase with larger magnetic fields. It may scale as B_0^2 or B_0 depending on the conditions of the plasma [16–18]. For our experiment the non–center-of-mass modes were not observed until times greater than 100 s.

Over long times, trapped plasmas have been observed to undergo a radial expansion resulting in a decrease in their aspect ratio and density with time and eventual gradual particle loss from the trap as the particles strike the ring electrode. In the absence of external torques, the total canonical angular momentum of the plasma is conserved [19], which places a limit on the radial expansion and the number of electrons that can be lost from the trap. Therefore, some external torque is responsible for this radial transport of particles and energy [20]. For experiments done in high vacuum apparatus (such as used here), the most likely candidates for this external torque are azimuthally asymmetric components in the trapping electric or magnetic fields [14]. Resonant enhancement of this transport rate can occur if the static field asymmetries couple to collective modes [3].

In thermal equilibrium, a cold electron (or ion) plasma with dimensions much less than those of the Penning-trap electrodes can be modeled as a uniform density spheroid which rigidly rotates about $\hat{z}$ at the rotation frequency ω_r, with $\omega_m\le\omega_r\le\omega_c'$ [3,4,21–23]. The density is $n_0=2\varepsilon_0m\omega_r(\omega_c-\omega_r)/q^2$ in the plasma interior and falls off at the plasma boundary over a distance approximately equal to the Debye length $\lambda_d=(\varepsilon_0kT/n_0q^2)^{1/2}$, where k is Boltzmann's constant, T the temperature, and ε_0 the permittivity of free space. For a comparison of experiment with theory, we will assume that the plasma is sufficiently cold that the Debye length is much smaller than the cloud dimensions. The plasma frequency ω_p, defined by $\omega_p^2=q^2n_0/m\varepsilon_0$, is related to the rotation frequency by $\omega_p^2=2\omega_r(\omega_c-\omega_r)$. The maximum density occurs for $\omega_r=\omega_c/2$, which is called the Brillouin limit.

The aspect ratio of the plasma, defined by $\alpha\equiv z_0/r_0$ with $2z_0$ the cloud length and $2r_0$ its diameter, is a function of the rotation frequency and therefore the density [23]. As $\omega_r\to\omega_c/2$ (Brillouin limit) the aspect ratio increases to its maximum value. If, in addition, $\omega_z\ll\omega_c$, the cloud is a long cigar shape (prolate spheroid) along z. For either $\omega_r\to\omega_m$ or $\omega_r\to\omega_c'$, α decreases and the cloud becomes a flat pancake shape (oblate spheroid). An exact expression relating α and ω_r is given in Refs. [4] and [23]. For $\alpha\ll1$, this expression can be expanded to first order in α with the result $\omega_p\simeq\omega_z(1+\pi\alpha/4)$.

We have neglected the effects of correlations in the plasma due to the electron/electron Coulomb interaction [24]. A measure of these correlations is the coupling constant $\Gamma\equiv q^2/(4\pi\varepsilon_0a_skT)$, where a_s is the Wigner-Seitz radius given by $4\pi a_s^3n_0/3=1$. For $\Gamma\ll1$, the plasma acts as a weakly interacting gas, so correlations can be ignored. For $\Gamma>1$, the plasma correlation increases and the plasma becomes liquidlike. As Γ further increases, the plasma crystallizes into a rotating lattice. In a Penning trap, the onset of crystallization has been directly observed using laser-cooled Be^+ ions [25]. A similar crystallization has also been reported in other systems, for example, in Paul traps [26], electrons on liquid helium [27], and, in the high-density limit, electrons in GaAs junctions [28]. For the work here, $\Gamma\simeq0.2$ was measured and therefore correlations can be ignored. In general, even in the presence of spatial correlations, if the electron/electron spacing is short compared to the wavelength of the modes, the plasma can be treated as a constant-density plasma.

The theory of the electrostatic fluid modes of a cold, constant-density, spheroidal plasma confined by a harmonic well was solved analytically for some simple cases in Refs. [3] and [4], and was solved for the general case by Dubin [2,4]. The theory, applied at the Brillouin limit, also applies to ion plasmas in the rf or Paul trap [4]. Dubin assumes that the plasma is in thermal equilibrium and its temperature sufficiently low that pressure effects can be ignored. In addition he assumes that a_s and λ_d

are much less than the plasma dimensions and the wavelength of the modes. By combining the continuity, momentum, and Poisson's equations, the differential equation for the electric potential was solved using scaled spheroidal coordinates. The solutions are a set of mode potentials expressed as products of associated Legendre functions P_l^m and Q_l^m and a factor $e^{i(m\phi-\omega t)}$, where ϕ is the azimuthal angle about the trap axis and ω is the mode frequency. Here l and m are integers which label the modes, with $l \geq |m|$. Without loss of generality, $m \geq 0$ may be assumed and negative frequencies allowed.

As examples of these modes [2–4] the $(l,m)=(1,0)$ mode is just the axial center-of-mass mode. There are two (1,1) modes which are just the magnetron and cyclotron center-of-mass modes, so all the $l=1$ modes are center-of-mass modes. The $l=2$ modes correspond to quadrupole deformations of the plasma shape. For example, there are two (2,0) modes. Here the plasma shape remains spheroidal, but the aspect ratio of the spheroid oscillates in time. The low-frequency (2,0) mode is a quadrupole oscillation where the axial and radial extents of the plasma oscillate out of phase with each other. The high-frequency (2,0) mode is similar, except that the axial and radial extents oscillate in phase as if the plasma were breathing. The three (2,1) modes are azimuthally asymmetric modes. For these modes, for small amplitude, the z axis of the plasma tips and precesses relative to the magnetic axis. In general, since the mode potential is proportional to $e^{im\phi}$, modes with $m=0$ are azimuthally symmetric while those with $m>0$ are azimuthally asymmetric. The (1,0) and (1,1) modes (center-of-mass modes) are commonly observed both with electronic and optical detection. The (2,0) and (2,1) modes have been observed using optical detection, and excitation of a (2,1) mode by a static field asymmetry was observed to heat the cloud [3].

A polynomial equation for the mode eigenfrequencies in a frame rotating at frequency ω_r is given in Eq. (5.13) of Ref. [4]. The mode frequencies in the laboratory frame are related to those in the rotating frame by $\omega_{l,m}(\text{lab})=\omega_{l,m}(\text{rotating})-m\omega_r$, where the term $m\omega_r$ is due to the Doppler shift. For $\omega_r \ll \omega_z \ll \omega_c$, the modes fall into three frequency ranges: high-frequency modes with $\omega \approx \omega_c'$, intermediate-frequency modes with $\omega \approx \omega_z$ (or ω_p), and low-frequency modes with $\omega \approx \omega_m$ (or ω_r). Because of our detection technique (described below), the modes which we detected were the intermediate-frequency modes. For ω_r, $\omega_z \ll \omega_c$ (the case here), they are magnetized plasma modes [4]. Here we summarize the $m=0$ and $m=1$ intermediate mode frequencies with $l-m \leq 7$ in the $\alpha \ll 1$ (low-density) limit. This was obtained by solving Eq. (5.13) of Ref. [4] for each value of l and m, to first order in α in the limit $\omega \approx \omega_p \ll \omega_c$ [29]. In the laboratory frame

$$
\begin{aligned}
|\omega_{1,0}| &= \omega_z \ , \\
|\omega_{2,0}| &= \omega_p \ , \\
|\omega_{3,0}| &= \begin{cases} \omega_z[1-\frac{5}{16}\pi\alpha] \\ \omega_p \ , \end{cases} \\
|\omega_{4,0}| &= \omega_p \ , \\
|\omega_{5,0}| &= \begin{cases} \omega_z[1-\frac{161}{256}\pi\alpha] \\ \omega_p \ , \end{cases} \\
|\omega_{6,0}| &= \omega_p \ , \\
|\omega_{7,0}| &= \begin{cases} \omega_z[1-\frac{969}{1024}\pi\alpha] \\ \omega_p \ , \end{cases} \\
|\omega_{2,1}| &= \omega_z \pm \omega_r - \tfrac{1}{8}\pi\alpha\omega_z \ , \\
|\omega_{3,1}| &= \omega_p \pm \omega_r \ , \\
|\omega_{4,1}| &= \begin{cases} \omega_z \pm \omega_r - \frac{29}{64}\pi\alpha\omega_z \\ \omega_p \pm \omega_r \ , \end{cases} \\
|\omega_{5,1}| &= \omega_p \pm \omega_r \ , \\
|\omega_{6,1}| &= \begin{cases} \omega_z \pm \omega_r - \frac{397}{512}\pi\alpha\omega_z \\ \omega_p \pm \omega_r \ , \end{cases} \\
|\omega_{7,1}| &= \omega_p \pm \omega_r \ , \\
|\omega_{8,1}| &= \begin{cases} \omega_z \pm \omega_r - \frac{8977}{8192}\pi\alpha\omega_z \\ \omega_p \pm \omega_r \ , \end{cases}
\end{aligned}
\tag{2}
$$

and in addition, for completeness,

$$
|\omega_{1,1}| = \omega_m, \omega_c' \ ,
$$

and to first order in α

$$
\begin{aligned}
\omega_p &= \omega_z[1+\tfrac{1}{4}\pi\alpha] \ , \\
\omega_r &= (\omega_z^2/2\omega_c)[1+\tfrac{1}{2}\pi\alpha] \ .
\end{aligned}
$$

The braces and $\pm$ signs indicate when there are more than one intermediate mode frequencies to first order in α. Notice that for all values of l and m (except for $l-m=1$) there are mode frequencies which decrease with decreasing α. In general, these frequencies occur for more than one mode; they are degenerate to first order in α. However, when $l-m$ is odd, there are also mode frequencies that increase with decreasing α. Each of these frequencies occurs for a single, nondegenerate mode. The center-of-mass modes (1,0) and (1,1) are independent of α and this the density of the cloud. However, (1) anharmonic terms in the trapping potential [$n>1$ in Eq. (1)], and (2) image charge shifts, which are neglected in these expressions, cause the c.m. frequencies to depend slightly on their amplitudes of oscillation as well as the spatial distribution of the plasma in the trap. As a result of these effects, as the plasma expands due to radial transport the c.m. mode frequencies will shift slightly.

By knowing ω_z and identifying and measuring the frequency of any non–center-of-mass mode (or alternatively by measuring the frequencies of any two non–center-of-

mass modes), the plasma's aspect ratio and therefore its rotation frequency and density can be calculated. We note that if modes that are azimuthally asymmetric ($m>0$) can be resonantly excited, then it might be possible to change the rotation frequency and increase or decrease the density. This is because the $m>0$ modes carry angular momentum. Therefore, by driving them it might be possible to apply to the plasma a torque which in turn could affect the plasma density.

The linewidths of the modes will be set by some combination of damping and dephasing processes. Mode damping could occur through resonant or nonresonant coupling to resistive elements making up the trap and support structure. Careful trap design can decrease (or increase) this loss mechanism. Coupling between electrostatic modes could also cause energy transfer out of any one mode, damping its amplitude. Landau damping of the modes has also been reported [7]. Dephasing of the modes, leading to line broadening, could occur because of small anharmonic terms in the trapping or mode potentials. In addition, electron/electron collisions could cause this dephasing.

II. EXPERIMENTAL APPARATUS

The trap used in this study was previously used to investigate the nonlinear excitation of a single trapped electron and the center-of-mass modes of electron clouds [30]. The trap electrodes (Fig. 1) were machined from oxygen-free copper and had an inner ring radius of 0.50 cm, resulting in $d=0.35$ cm. When a voltage V_0 was applied between the endcaps and the ring, the resulting electric potential near the trap's center closely approximated a harmonic potential along the z direction (with $c_2=0.487$) [31]. The cylindrical symmetry of the electrodes minimized azimuthally asymmetric electric perturbations. The leading order perturbation to the potential was the term labeled by c_4 in Eq. (1). However, by applying a voltage V_g to the additional guard electrodes [32] and observing the axial c.m. mode line shape, this perturbation could be reduced to $|c_4|\leq 5\times 10^{-5}$. For a precision hyperbolic trap without guard electrodes, typically $|c_4|\geq 10^{-3}$ [11]. The ring electrode was split into three sectors (Fig. 1). Typical operating parameters for this trap were $V_0=-10.45$ V, $B_0=0.110$ T, $\omega_z/2\pi=61.54$ MHz, $\omega_m/2\pi=615.0$ kHz, and $\omega_c'/2\pi=3.079$ GHz.

The magnetic field B_0 was produced with a multifilament Nb-Ti superconducting magnet. The field homogeneity near the trap center was specified as $\Delta B/B_0\leq 2\times 10^{-5}$ for a 1-cm-diam volume. The magnetic field's long term drift was measured to be within 1×10^{-5}/h–7×10^{-7}/h for $B_0=0.1$ T. The trap was mounted at the center of the magnet in a sealed copper vacuum container. The magnet and vacuum container shared a common liquid-helium bath. The large cryosorption rate of the liquid-helium cooled walls maintained the vacuum inside the trap. The background pressure in a similar system was measured to be less than 7×10^{-15} Pa (5×10^{-17} Torr) [33]. An additional set of Helmholtz coils whose axis was perpendicular to B_0 and whose center was common with the trap center was mounted external to the magnet dewar. These coils were used to minimize the angle Θ_0 between the trap magnetic and electric axes when $B_0\simeq 0.1$ T.

Electrons were loaded into the trap by using a field-emission point (FEP) aligned along the $\hat{z}$ axis and mounted in one endcap. By applying a negative potential of 600 V to the FEP an electron beam which passed into the trap and back out through matching holes in the endcaps was formed. Inside the trap the electron beam ionized background gas, which in turn supplied the low-energy secondary electrons which were trapped. By varying the beam current, the loading rate was varied from 0.01 to 100 s^{-1}.

The electronic system (Fig. 2) used to detect the signal induced by the electron's motion was similar to that developed at the University of Washington [10,11,34,35]. At the heart of the system is a helical resonator tuned circuit (TC) with frequency ω_{TC}. The resonator is attached to one endcap and its frequency set such that $\omega_{TC}\simeq\omega_z$. The current induced in this endcap by the electrons' axial motion produces a voltage drop across the tuned circuit which was then amplified with a dual gate GaAs FET preamplifier. Both the tuned circuit and preamplifier were immersed in the liquid helium. The real part of the tuned circuit impedance sets the damping rate and

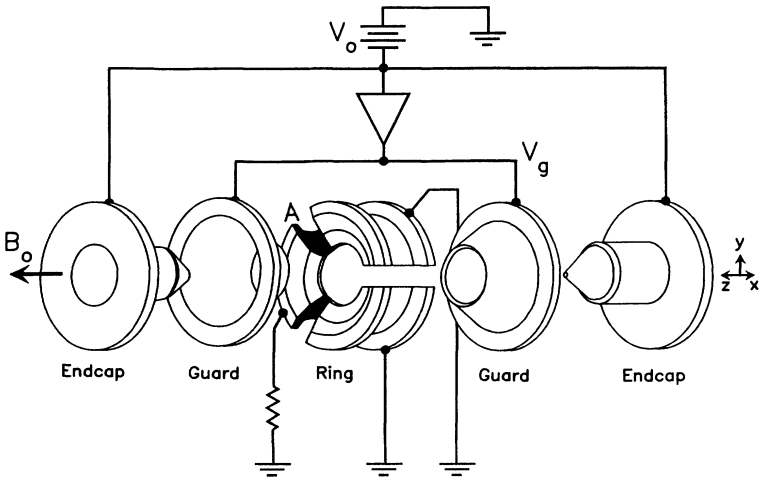

FIG. 1. A schematic diagram of our Penning trap. The electrodes have been separated along the axis to show details. The inner ring diameter is 1 cm.

linewidth of the axial c.m. motion [10,11,36]. The axial c.m. linewidth $\Delta\omega_z$ for our experiment was $\Delta\omega_z = N \times 19$ s^{-1} for $\omega_z = \omega_{TC}$, where N was the number of electrons. Therefore, an estimate for the number of electrons trapped was made by measuring $\Delta\omega_z$. The thermal amplitude of the axial c.m. motion (and the cyclotron c.m. motion via synchrotron radiation) had a characteristic temperature set by the liquid-helium bath, $T = 4$ K.

Different detection methods were used in this study. The following is a brief description of each.

1. Noise power. In this detection method the noise induced in the endcap by the electrons' thermal motion was detected using a spectrum analyzer which acted as a square-law power detector [34,36]. When this spectrum analyzer was used to detect noise near the axial c.m. frequency, a noise decrease (or "dip") was observed for $\omega_z \simeq \omega_{TC}$ as the electrons short circuited the tuned circuit's noise voltage [36]. A noise peak occurred for values of ω_z outside of the tuned circuit resonance [36]. The advantage of this detection technique was that it was passive, requiring no oscillating drive voltages to be applied to the trap.

A related detection method is sometimes called the "bolometric" method [6,34,36,37]. In this method, the spectrum analyzer's local oscillatory frequency is fixed so that only noise power around ω_z is observed. A parametric drive at $2\omega_z$ can be applied to heat the cloud increasing collisions and coupling between the modes. An oscillating drive voltage at frequency $\omega_d \neq \omega_z$ can simultaneously be applied to any of the trap electrodes. If the electrons absorb energy at ω_d, and if some of this energy is coupled through some mechanism to the axial c.m. motion at ω_z, then an increase in the noise is observed.

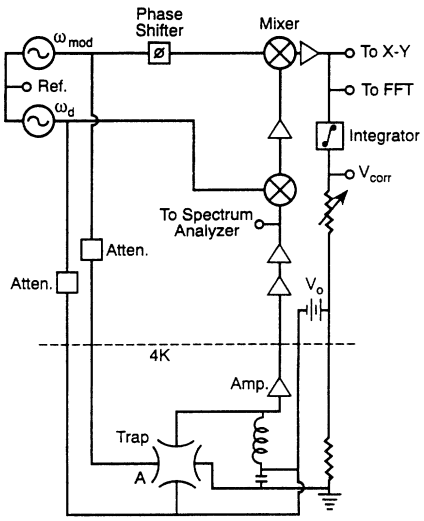

FIG. 2. A schematic diagram of the electronic detection system used in detecting the electrostatic modes of the electron plasma. The primary detection method was to look at the noise induced in one endcap using the spectrum analyzer, with the voltages at ω_d and ω_{mod} set to zero amplitude. In addition, the response of the plasma to the coherent drives ω_d and ω_{mod} was also detected and recorded by the X-Y recorder. A dynamic signal analyzer which recorded the fast Fourier transform (FFT) of the response was used as a diagnostic tool. V_{corr} is the servomechanism correction voltage.

2. Coherent. In this method, typically, the electrostatic well is modulated at a frequency $\omega_{mod}/2\pi = 1$ MHz producing frequency modulation sidebands on ω_z. A second drive of frequency ω_d is then applied to an endcap with $\omega_d \simeq \omega_z + \omega_{mod}$. As ω_d is swept through resonance with the sideband ($\omega_d = \omega_z + \omega_{mod}$), the electrons' axial c.m. is excited, and this excitation is turn induces a signal in the other endcap near ω_z. This signal is then amplified and phase-sensitively (linearly) detected with a double-heterodyne receiver [10,11,35]. The modulation allows the drive to be applied at a frequency different than ω_{TC}, thus preventing saturation of the preamplifier. This method is very sensitive to small coherent changes in the axial c.m. amplitude.

3. Axial frequency shift. Because of imperfections in the static trap fields ($c_{2n} \neq 0$ for $n > 1$, and B_0 not homogeneous) and because of relativistic effects, the axial c.m. motion is slightly anharmonic and weakly coupled to the other degrees of freedom [10,30,38]. As an example, the axial c.m. frequency ω_z becomes dependent on the amplitude of oscillation of the c.m. magnetron motion. If the magnetron motion is excited, the axial frequency shifts because of the residual c_4 term in the trap potential. For a change of $r_m = 0 \rightarrow r_{m0}$ in the magnetron amplitude, the axial frequency shifts by $\delta\omega_z/\omega_z \simeq 3c_4 r_{m0}^2/(2c_2 d^2)$. To observe the axial frequency shift, an electronic servomechanism is used [10,38]. An axial drive is used to weakly excite the axial c.m. motion. The response to this drive is then detected and the output of the coherent phase detector is integrated and added (fedback) to V_0 with the correct sign. This effectively locks the axial frequency, holding it fixed relative to the (synthesized) drive and modulation frequencies. Any effect which would otherwise change the axial c.m. frequency is observable by monitoring the correction signal of the servo.

An additional experimental technique which was investigated was a parametric mode-coupling technique called magnetron sideband cooling [10,11,39], which is analogous to laser cooling [40]. It was first reported in experiments involving single electrons at the University of Washington [10]. The technique is used to reduce the metastable magnetron c.m. amplitude by parametrically coupling this motion to the axial c.m. motion which is damped by its coupling to the tuned circuit ($\omega_z = \omega_{TC}$). This parametric coupling is accomplished by applying a spatially inhomogeneous electric potential of the form $\phi(x,y,z) = V_p xz \cos(\omega_z + \omega_m)t$. The magnetron amplitude can be damped to a theoretical limit given by $r_m = 2[(\omega_m/\omega_z)\langle r_z^2 \rangle]^{1/2}$, where $\langle r_z^2 \rangle^{1/2}$ is the thermalized axial amplitude. Similarly, the magnetron motion can be damped through coupling to the cyclotron motion. Theoretical models of the cooling have not included plasma effects [11,39,41], although plasma models for parametric couplings between plasma modes might apply [42]. Evidence that sideband cooling affects the radial transport rate of a plasma has been found previously, in that, with the cooling on, cloud lifetimes are extremely long [33]. However, the effect of sideband cooling on the

aspect ratio and density of a plasma has not been studied before. For our trap the sideband cooling drive was applied to the ring sector A. The necessary axial dependence to the drive arose from the different impedances attached to the endcaps.

III. EXPERIMENTAL RESULTS

A. Observation of the modes from the noise power

Detection of the noise power of the induced currents in one endcap (method 1 above) gave the most definitive results, so we focused our attention there. After a cloud of electrons was loaded and the field emitter (and all drives) turned off, the axial c.m. motion with frequency $\omega_z=\omega_{1,0}$ could be seen in the noise spectrum (see inset in Fig. 3). Initially, the frequency of the c.m. motion decreased slightly with time. At a later point in time, noise peaks began to appear in the noise spectrum (Fig. 3). The frequencies of these noise peaks increased in time, with some crossing the axial c.m. frequency and others approaching it asymptotically (Fig. 4). If $\omega_z=\omega_{TC}$, so the axial c.m. signal was a noise dip, then as the peaks approached ω_z they too would change to noise dips, then back to peaks after the crossing. After the last crossing, the frequency of the axial c.m. mode would begin to increase slightly. Eventually, one by one, the amplitudes of the peaks decreased until they were no long observable, with the axial c.m. mode typically the last to be seen. Surprisingly, it was found that the larger the value of $|c_4|$ the smaller the absolute frequency shift of the axial center of mass.

The number of noise peaks which were observed depended most strongly on the number of electrons in a cloud. For clouds of 7000 electrons only the c.m. signal and one other peak were observed. For clouds of 70 000 electrons as many as ten peaks besides the axial c.m. peak were observed. The time at which the first additional noise peak appeared was found to be strongly dependent on the magnetic-field strength B_0. For $B_0=0.11$, 0.25, and 1.4 T (and for all N between 7000 and 70 000) the first peaks (other than the $\omega_{1,0}=\omega_z$ mode, which was seen immediately) appeared at the respective average times 520, 2000, and 15 800 s after loading. The modes were observed as the clouds' aspect ratio decreased below $\alpha\approx 0.02$. It was likely that the magnetic-field dependence was partly due to a slower radial expansion with larger magnetic fields. Also, the larger magnetic fields should have produced a more tightly confined electron beam that was used to load the electrons. This probably resulted in an initial cloud of smaller radial dimension.

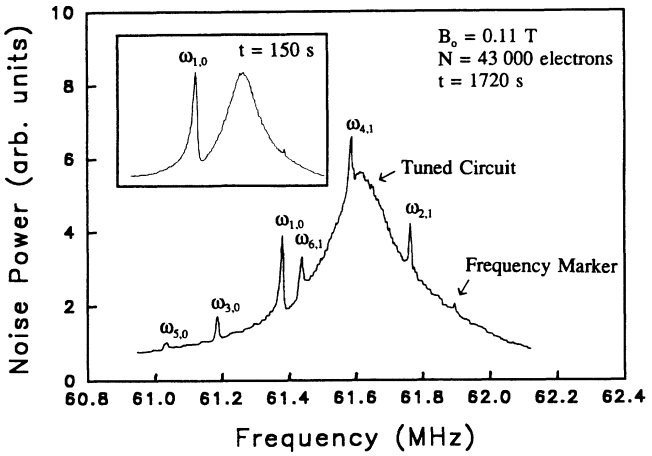

FIG. 3. The noise spectrum induced in one endcap as seen by the spectrum analyzer (resolution bandwidth is 10 kHz). The broad peak centered at 61.6 MHz is the axial tuned circuit resonance excited by thermal ($\simeq$4 K) noise. The inset shows the noise spectrum of a newly loaded cloud ($t=150$ s after loading) in which only the axial center-of-mass mode and tuned circuit resonance are seen, and with ω_z slightly detuned from ω_{TC}. In the main figure the signals from six electrostatic modes including the axial center of mass mode can be seen at a later time ($t=1720$ s after loading). Here $B_0=0.11$ T.

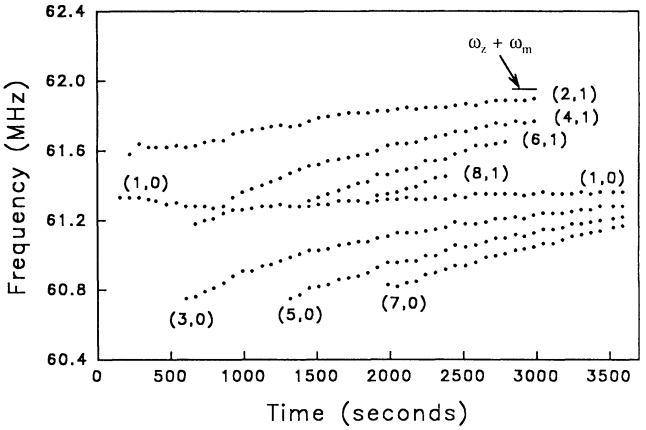

FIG. 4. A plot of the frequencies of the modes vs time after the cloud was loaded. The modes are labeled by their (l,m) values. These data were taken using a spectrum analyzer and were from the same data set as in Fig. 3. For these data the sideband cooling was off and the guard electrode voltage detuned so that $|c_4|\simeq 4\times 10^{-3}$. The measurement uncertainty in the frequency is less than the symbol size used in the plot and is the same for all points.

Figure 4 shows a plot of the frequency of the noise peaks, including the axial center-of-mass peak, as a function of the elapsed time after an electron cloud was loaded into the trap. As discussed above, the frequency of the center-of-mass peak decreased slightly for early times after loading and then increased slightly. The figure shows two sets of noise peaks: those which asymptotically approach the axial center-of-mass frequency ω_z and those which asymptotically approach $\omega_z+\omega_m$. These peaks can be identified with some of the electrostatic mode frequencies of Eq. (2) for a pancake shaped (strongly oblate) plasma ($\alpha\ll 1$). The peaks which asymptotically approach ω_z can only be $m=0$ modes. The peaks which asymptotically approach $\omega_z+\omega_m$ can only be $m=1$ modes. In addition to the noise peaks shown in Fig. 4, some peaks were observed at early times and appeared to be $m=2$ modes. These modes were only detected for a brief time which made their identification uncertain.

As discussed previously, azimuthal asymmetries in the trap cause a radial expansion of the plasma. The radial expansion should produce a decrease in the plasma's aspect ratio with increasing time. Therefore the mode frequencies detected in Fig. 4 apparently increase with decreasing aspect ratio (except the center-of-mass mode, whose frequency remains relatively constant). From Eqs. (2), only the frequencies of a subset of the modes with $l-m$ odd increase, or stay the same, for decreasing aspect ratio. For modes in this subset with $m=0$, the (1,0) mode has the highest frequency, the (3,0) mode has the next highest, the (5,0) the next, etc. For modes in this subset with $m=1$, the (2,1) mode has the highest frequency, the (4,1) the next highest, etc. In this manner, we were able to make the probable identification shown in Fig. 4 of the noise peaks.

The modes can be used to obtain information on the aspect ratio as a function of time. Following Dubin's cold fluid theory, we let $\omega_{1,0}$ be an estimate of ω_z. (This means our estimate of ω_z varies slightly as a function of time which disagrees with the ideal cold fluid theory.) Then, from Eqs. (2), every non-c.m. mode which we detected provides an estimate for the plasma aspect ratio α. Figure 5 shows the estimated aspect ratio as a function of time from the data of Fig. 4, using the measured value $\omega_c/2\pi=3080$ MHz. Fair agreement between the different estimates is obtained. Excluding the $\omega_{2,1}$ mode estimate, all the other estimates agree to better than 20%. It appears that the differences between the estimates are due to a systematic effect not included in the theory. In Fig. 5(b) it is seen that the estimated aspect ratio depends on $l-m$. As $l-m$ increases, the estimated aspect ratio decreases. For example, the (2,1) mode gives the highest estimated aspect ratio. The aspect ratio estimates from the (4,1) and (3,0) modes agree, but are less than the (2,1) estimate, and they are in turn greater than the (6,1) and (5,0) estimates. If the systematic dependence of the aspect ratio estimates on $l-m$ could be corrected, it appears that the mode frequencies could be used to calculate the plasma aspect ratio to better than 5%. We also note that the noise fluctuations in the estimates for the plasma aspect ratio decrease with increasing $l-m$. This is a result of the different sensitivities of α to the different mode frequencies [see Eqs. (2)].

The systematic shifts in the mode frequencies can also be seen in Fig. 4. From Eqs. (2), the intervals in Fig. 4 between neighboring $m=0$ noise peaks and also between neighboring $m=1$ noise peaks should equal $\omega_z\alpha$ to within a few percent. A visual inspection of Fig. 4 shows that the differences in these intervals are not equal within a few percent. In general, the intervals decrease in frequency as l increases. The smallest frequency intervals are 25–30% less than the largest frequency intervals. Similar results are found for $|c_4|<5\times10^{-5}$. The discrepancy between the detailed predictions of Eqs. (2) and the observed noise peak frequencies of Fig. 4 may be due to (1) coupling of the modes with each other causing relative frequency shifts, (2) shifts due to image charges because the plasma radius is approaching the ring radius, and (3) the small thickness of the cloud. Because the detected modes appear to be two dimensional (discussed

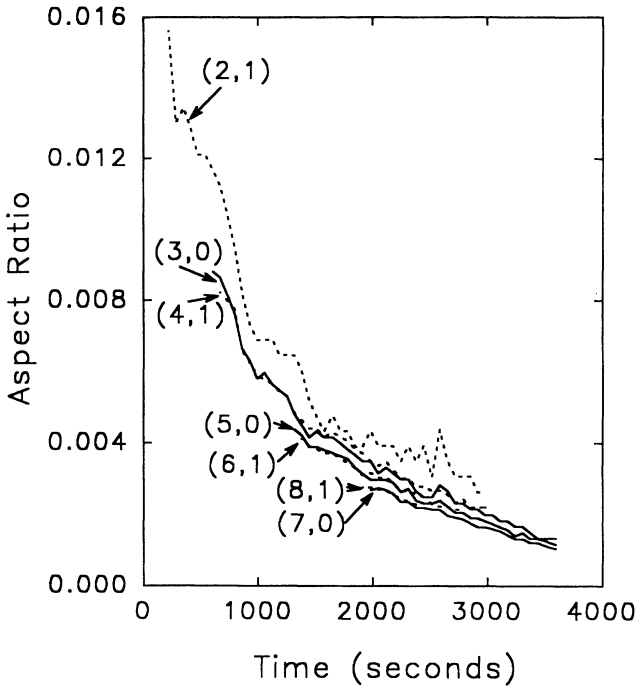

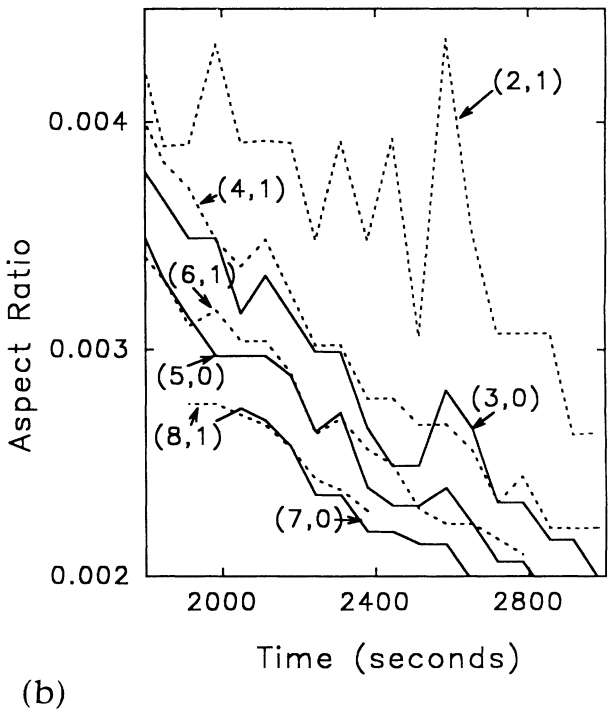

FIG. 5. (a) Estimates of the cloud aspect ratio α as a function of the time since the cloud was loaded, for the data of Fig. 4. For each time, the (1,0) mode is used to estimate ω_z. Each (l,m) mode is then used to provide an estimate for α. The calculated values for α have been connected by straight lines for each mode. The values of α from $m=1$ ($m=0$) modes are connected by dashed (solid) lines. (b) An expanded view of (a) from 1800 to 3000 s showing the systematic dependence of the estimated aspect ratios on l and m.

below) the small thickness of the cloud should be less important. Evidence for the mode coupling is discussed below. The frequency variation of the (1,0) mode is possibly due to a combination of mode coupling, anharmonic effects, and image charge effects. If the size of the frequency variation of the (1,0) mode is used as an estimate of potential systematic shifts, then these shifts are sufficient to explain the apparent differences in the intervals between the mode frequencies.

As an example of what the mode frequencies infer about the plasmas, from Fig. 5 at time $t=1720$ s, we find that $\alpha=0.0039\pm0.0005$. The uncertainty here is equal to the scatter between the average aspect ratio estimate and the individual estimates. From the linewidth of the $\omega_{1,0}$ mode for $\omega_{1,0}=\omega_{TC}$ when first loaded, we determined $N=43\,000$. The calculated electron density is then 4.7×10^7 cm^{-3}, which implies an interparticle spacing of 17.2 μm and cloud dimensions of $z_0=14.9$ μm and $r_0=3830$ μm. Assuming the plasma was thermalized to $T=4$ K, the Debye length was $\lambda_d=20.1$ μm and the coupling strength was $\Gamma=0.24$.

The evolution of the mode frequencies was studied while varying different trap parameters. As discussed above and below, the two parameters which had the most profound effect on the plasma in this low-density limit were the magnetic-field strength and the application of a cooling drive. The appearance time of the mode peaks depended strongly on B_0 (the trap axial frequency was kept constant for all B_0). For all B_0, the signals from the modes appeared when the plasmas' aspect ratios were approximately the same, $\alpha\simeq0.02$. This means the mode frequencies for different B_0 were also about the same. However, the rate at which the frequencies of these peaks changed in time due to radial expansion was found to be fairly insensitive to B_0 (see Fig. 6). This needs to be studied in more detail with better control over all other experimental parameters (such as Θ_0). Increasing the number of trapped electrons from 7000 to 70 000 had little effect on the mode evolution. Changing the trap angle from $\Theta_0<0.030°$ to $\simeq0.7°$ (increasing the azimuthal asymmetry), distorting the electrostatic well by adding to 0.5 V to ring sector A (again, increasing the azimuthal asymmetry), or decreasing the resistance to ground of sector A from 105 to 16 Ω (which might change the radial damping) also had little or no effect on the mode evolution. Changing the guard voltage so that the trap was less harmonic (larger $|c_4|$) allowed the modes to be observed for a longer time after they appeared. It also slowed the rate of change of the aspect ratio, but by only a factor of 2.5 for a change of $|c_4|\leq5\times10^{-5}$ to 4×10^{-3}. Having the cooling drive on or off during the initial loading had no effect on the mode evolution, nor did having ω_z tuned or detuned from ω_{TC}. We also tried to change the plasma's density by applying a drive to ring sector A resonant with the azimuthally asymmetric ($m>0$) modes whose frequencies were near ω_z. No change in the mode frequencies was observed. Of these different control parameters, the only one which had any dramatic effect on the signal size, or number of observed modes, was the number of electrons in the plasma. We found that (as noted above) the larger the number of electrons, the larger the number of modes that were observed.

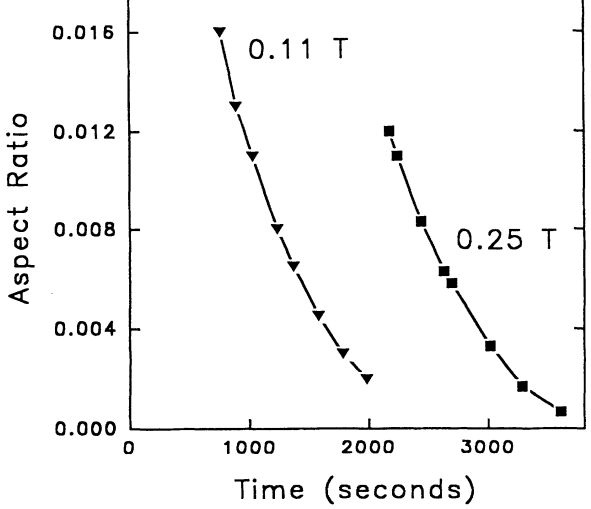

FIG. 6. The evolution of cloud aspect ratio as calculated from the frequencies of the $\omega_{3,0}$ mode and ω_z for two different magnetic fields. For $B_0=0.1$ T, $N=43\,000$ electrons and $\Theta_0\leq0.03°$; and for $B_0=0.25$ T, $N=57\,000$ electrons and $\Theta_0\simeq0.7°$.

As mentioned previously, we detected only a subset of all of the possible modes with frequency near ω_z. Why we observed these modes and not others involves a number of factors. We found that by inspecting the mode potential [4] that the modes detected in Fig. 4 look like drumhead modes of a two-dimensional disk. At a given radius and azimuthal coordinate, all the electrons of the plasma oscillate axially in phase. Parts of the plasma with different radial positions and azimuthal coordinates oscillate with different phases. These modes are two dimensional and will exist in the limit that the thickness of the electron plasma is much less than the mean interparticle spacing. Modes which we did not detect have structure in the axial direction (the phase of the motion depends on z) which can be characterized by an effective wavelength which is less than, or on the order of, the plasma's axial extent. The continuous, fluid description of these modes breaks down when the interparticle spacing is comparable to or larger than this wavelength. In particular, when the plasma is very thin it is not clear how to think about these modes, and their calculation from the formulas of Refs. [2] and [4] is not correct.

In order to understand some of the other factors that determined which modes we observed, we require a better understanding of the detection mechanisms. There are at least two mechanisms by which the modes could couple to the endcap and be detected. The first is that, like the axial center of mass, the modes couple directly to the endcap by electrostatic coupling [6,43]. In general, the efficiency of inducing axial currents in the endcap depends on the radius of the plasma. Therefore, modes whose radial extent is on the order of r_t might induce a detectable current in the endcap even though the net axial velocity of the plasma is zero. For detection of an azimuthally asymmetric ($m>0$) mode this requires that the cylindrical symmetry of the trap be broken by, for ex-

ample, a misalignment of the trap's electric and magnetic axes [44].

A second coupling mechanism for detection would be that the modes couple directly to the axial c.m. mode, which in turn couples to the endcap. This coupling could be by field asymmetries or mediated by image currents induced in the electrodes. For an ideal trap, small plasma size, and low mode excitation, all the modes are independent and therefore there would be no such coupling between the modes. However, Fig. 7 shows a narrow frequency span as the frequencies of two of the modes intersect that of the axial c.m. The (2,1) mode forms an anticrossing (or avoided crossing) with the axial center-of-mass mode; the mode frequencies never overlap. This is a general characteristic of two coupled oscillators [45]. Further evidence of the mode coupling was observed in the mode linewidths. Modes with frequencies different from ω_z by more than 150 kHz had full width at half maximum (FWHM) linewidths less than 10 kHz. These linewidths were observed to increase as the mode frequencies approached ω_z, as would be expected since the axial center-of-mass linewidth was larger.

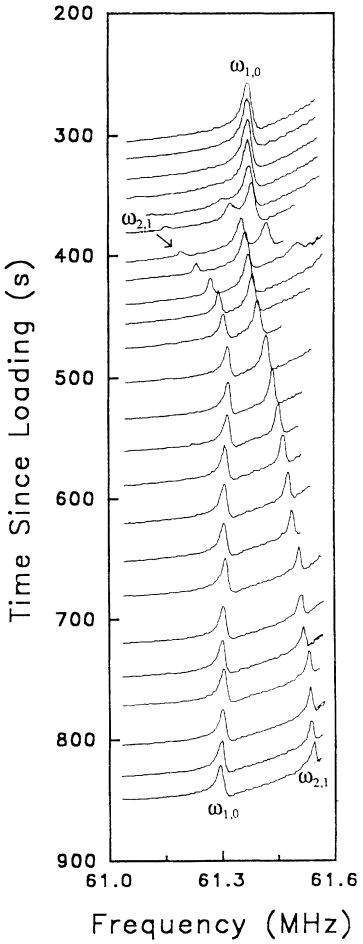

FIG. 7. A series of noise spectra (as in Fig. 3) of a cloud of 20 000 electrons (with $|c_4| \leq 5\times10^{-5}$, $B_0=0.11$ T) showing an avoided crossing between the axial center-of-mass mode and the ω_{21} mode (plus an avoided crossing of an unidentified mode at $t\approx380$ s). As the modes approach each other they couple together resulting in the mode frequencies never becoming equal. The modes were identified by observing their behavior after the cloud was first loaded and also their asymptotic behavior for long times. The resolution bandwidth is 10 kHz.

These two detection mechanisms are not completely independent, making it difficult for us to differentiate between them. In addition, we might observe the modes through a combination of the two mechanisms. Additional evidence comes from the fact that we did not detect the $m=1$ subset of modes whose frequencies went as $\omega_z-\omega_m-k(l)\alpha$, where $k(l)$ is a constant which depends on l [see Eq. (2)]. This was true for both $\omega_z-\omega_m\approx\omega_{TC}$ and $\omega_z-\omega_m<\omega_{TC}$. These modes have the same mode potential as the subset of modes whose frequencies went as $\omega_z+\omega_m-k(l)\alpha$, which we did detect. However, this subset of modes which we did detect crossed or had a small detuning from ω_z, while the others did not. Another important factor was that, when we purposely increased the trap azimuthal asymmetry (as discussed above), the signal size and number of observed $m=1$ modes did not noticeably increase. Also, when we increased $|c_4|$ we were able to observe all the modes for a longer time. Together, these observations imply that coupling to the axial c.m. mode might have been the more important detection mechanism for us.

B. Effect of sideband cooling

The effects of sideband cooling were studied by first loading a cloud and allowing it to evolve to the point where some of the other modes besides the axial c.m. mode were observed. Then a strong sideband cooling drive was applied with frequency $\omega_z+\omega_m$ (for $\omega_z\simeq\omega_{TC}$). After a few seconds, all the modes other than the c.m. mode disappeared. In addition, the c.m. mode frequency was back to its initial loading value. If the drive was then turned off, the other modes reappeared in approximately the same time, and in the same order, as a newly loaded cloud. This process was found to be very repeatable. Each time after the strong cooling drive was applied, the mode frequencies evolved at the same time and rate as that of a newly loaded cloud, except that the time was measured from when the drive was turned off. Thus, after each time the cooling was applied, the plasma density was reset back to the same value. Electrons were lost only when the cloud was allowed to expand radially until they struck the ring electrode before the cooling drive was applied. The point at which electrons began to be lost was consistent with the ring electrode radius being equal to the cloud radius as calculated from the mode frequencies. A typical drive strength to observe the effect of the sideband cooling drive was $V_A/V_0\simeq10^{-4}$ at ring sector A for 10 000 electrons and $B_0=0.1$ T, where V_A is the voltage on A. Similar results were found for the different magnetic fields used, as well as with the cooling drive applied at frequency $\omega_d=\omega_z+2\omega_m$ with a larger drive amplitude. With a weak cooling drive on continuously, additional modes were observed in the noise spectrum but they were not positively identified.

From these observations we conclude that the sideband cooling not only can stop radial expansion, but can reverse it by increasing the rotation frequency, and thus the aspect ratio and density, of the cloud. The rotation frequency was increased to approximately the same value as

the loading value. Applying the drive after the cloud expanded increased the aspect ratio by more than a factor of 20 from $\alpha < 0.001$ to $\alpha > 0.02$. For our conditions this implies an increase in the density of $\geq 3\%$. The mechanism for this compression of the cloud and what determines the limit to that compression are not known. One possibility is that the parametric coupling directly reduces the magnetron center-of-mass amplitude just as for a single electron. Then, anharmonic terms in the trapping potential might couple the magnetron c.m. mode to other non-c.m. modes [36] resulting in a compression. A second possible mechanism is that the parametric drive directly couples some other azimuthally asymmetric mode whose frequency is close to ω_m (like the lower frequency $\omega_{2,2}$ mode) to the axial center-of-mass mode. The cooling would then proceed until the azimuthally asymmetric mode frequency had shifted away from the resonance condition as the plasma density increased. Both of these mechanisms are possible in that we observed: (1) apparent electrostatic coupling between c.m. and azimuthally asymmetric non-c.m. modes (see Fig. 7) and (2) parametric coupling between a c.m. and an azimuthally asymmetric non-c.m. mode (discussed below).

C. Alternate detection methods

Detection of non-c.m. modes was also possible using the other techniques discussed in Sec. II. The "bolometric" technique (described in method 1 above) did not detect any modes, but it was not thoroughly tested. However, by using coherent detection (method 2 above) some of the modes were detected. Figure 8 shows the output of the phase-sensitive detector when the drive frequency was swept through $\omega_z + \omega_{\text{mod}}$. Two modes besides the axial c.m. mode are seen in the figure. This demonstrates that not only can we detect these modes coherently, but also that we can excite them with external drives.

Figure 9 shows the servo correction voltage in the axial frequency shift detection method (method 3 of above). Here the axial c.m. frequency was kept fixed by the servomechanism while a drive was applied to ring sector A. For $B_0 = 0.1$ T, a resonance appeared when the drive frequency was between ~ 100 and 500 kHz, and the resonance had a dispersive line shape. As time increased, this resonant frequency increased, always staying below ω_m. The resonance was very repeatable from cloud to cloud and was observable on clouds with as few as 300 electrons. As the drive strength was increased, the line shape became hysteretic, depending on the direction that the drive frequency was swept and the amplitude of the drive.

Evidence for the origin of this resonance was found when we simultaneously detected both the noise spectrum (method 1) and the axial frequency shift (method 3). We found that the resonant frequency of the dispersive resonance occurred at exactly the measured difference frequency between $\omega_z = \omega_{1,0}$ and $\omega_{2,1}$ for all the time the resonance could be observed. However, this dispersive resonance could be observed only after the $\omega_{2,1}$ mode had crossed over ω_z. Apparently the drive was capable of parametrically coupling together the (2,1) mode and the

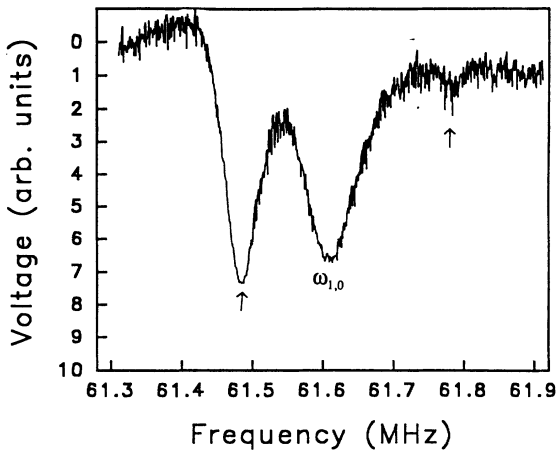

FIG. 8. Data taken using coherent detection (method 2 in the text) with $\omega_z \simeq \omega_{TC}$ and a detection bandwidth of 10 Hz. The axial potential well was modulated at $\omega_{\text{mod}}/2\pi = 1$ MHz. A coherent drive applied to one endcap was swept across $\omega_z + \omega_{\text{mod}}$ and the response detected phase sensitively in the absorptive mode. These data were taken for $B_0 = 0.11$ T, $N = 26\,000$ electrons, and $|c_4| < 5 \times 10^{-5}$. The signals from the axial center-of-mass plus two other modes can be seen.

axial c.m. mode, similar to magnetron sideband cooling. This was done either directly by the parametric electric field or indirectly through the field's modulating the coherent axial motion necessary for the detection. This mode coupling might also explain the dispersive line shape since, as the modes become more strongly coupled

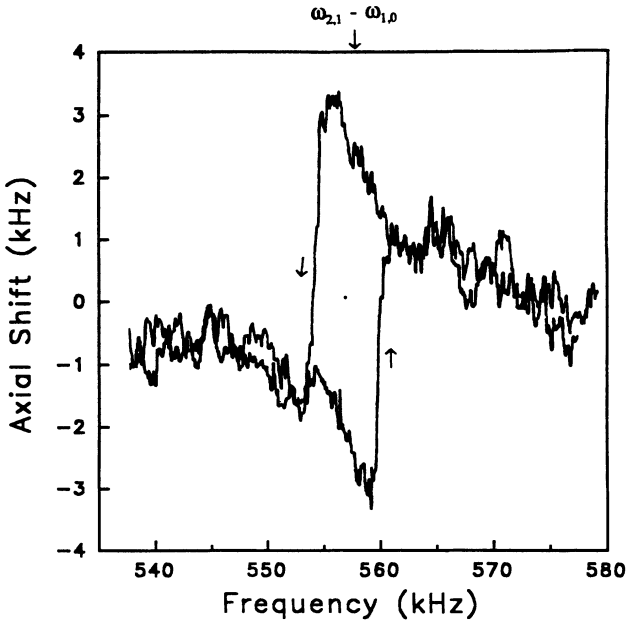

FIG. 9. The detection of the $\omega_{2,1}$ mode by monitoring the correction voltage to the locked axial center-of-mass frequency when a spatially inhomogeneous drive was applied through ring sector A and its frequency swept through $\omega_{2,1} - \omega_z$ (method 3 in the text). These data were taken for $B_0 = 0.11$ T, $N = 3000$ electrons, $|c_4| < 5 \times 10^{-5}$, and $\omega_m/2\pi = 615$ kHz. The arrows show the direction of the sweep. The hysteresis in this dispersive resonance can be seen. For sufficiently hard drives, the axial frequency could be shifted by much more than its linewidth.

together by the field, the modes would form an avoided crossing [45]. Our detecting just the frequency of the axial c.m. mode, while varying the coupling by sweeping the drive frequency, would result in a dispersive line shape. This line shape would become more hysteretic the stronger the coupling strength.

IV. DISCUSSION AND CONCLUSIONS

We have shown that it is possible to detect the electrostatic modes of a pure electron plasma in a Penning trap using nondestructive electronic methods. We detected several azimuthally symmetric and asymmetric modes in the low-density limit where the plasma approaches a two-dimensional charged disk. We observed these modes in the low-density limit because the noise power detection technique which we primarily used is facilitated by the mode frequencies being close to the axial center-of-mass frequency. This occurs for the intermediate frequency modes when the plasma density is low. We found that the frequencies of these modes fit Dubin's theoretical model [2,4] reasonably well. Also, we found that we could excite these modes directly with external drives, and in addition, by parametrically coupling modes together. The observation of these modes allowed the rotation frequency, shape, and density of the plasma to be determined. From auxiliary measurements of the electron number, we could then determine the plasma size. The detection techniques demonstrated here should work for any type of non-neutral trapped plasma, and should be applicable to the detection of modes other than the intermediate frequency modes. Other modes might also be detectable with a different geometry of electrodes to act as induced current detectors. The modes observed here may correspond to some of the features reported by Barlow [6], but a comparison is difficult because of differences in the detection.

In studying these modes we also observed behavior which departed from Dubin's model. This included a time dependence to the axial center-of-mass mode frequency due in part to the plasma radial expansion in an anharmonic trap. Also, we observed coupling between the axial center-of-mass mode and other modes evidenced, primarily, by avoided crossing behavior as their frequencies became degenerate. It is likely that this coupling is one cause for the deviations between observed and predicted mode frequencies, and will have to be studied further in order to get a more complete picture of the plasmas' characteristics. In addition, in comparing our data with Dubin's theory we found there to be a systematic shift in our measured aspect ratios as a function of $l-m$ where (l,m) is the mode used to determine the aspect ratio. To be able to measure plasma aspect ratios to much better than 20% will require this systematic effect to be understood and corrected for.

We also demonstrated that the parametric coupling technique called magnetron sideband cooling, which couples the magnetron and axial center-of-mass motions, not only stops the radial expansion of the plasma, but actually compresses the plasma increasing its density. The mechanism for this compression needs to be found in hopes of achieving higher densities with this technique. An interesting test would be to look for compression by sideband cooling when the coupling is between the magnetron and cyclotron motions. The ability to control the density without requiring optical methods might open new avenues for the study of cold non-neutral plasmas in Penning traps.

This study leaves a number of issues to be investigated. While the origin for the coupling between modes might be related to static electric field asymmetries, this needs to be studied further. Also, the mechanisms by which the modes are detected need not be positively identified. A detailed study of the signal amplitudes and linewidths of the modes would be a helpful first step towards solving these problems. A detailed study of the linewidths might also yield information on electron/electron collisions in trapped plasmas. If trapped, strongly coupled electron plasmas could be achieved, then these mode linewidths might be a measure of spatial correlations in the plasma. For example, in experiments on electrons localized near the surface of liquid helium, it has been demonstrated that the linewidth of shear wave resonances depended on Γ [46]. Similar results have been predicted for the electrostatic mode linewidths discussed here [47].

One important plasma parameter which we could not easily control was the plasma temperature T. Other groups have controlled their ion and electron plasmas' temperatures by introducing a buffer gas (e.g., Refs. [7], [43], and [48]). This has the disadvantages of applying an external torque on the cloud causing it to expand, being limited to temperatures greater than 4 K, and introducing what can be undesirable ion/neutral collisions affecting the physics to be studied. The problem of radial expansion due to the torque applied by the buffer gas can be eliminated by applying simultaneously a sideband cooling drive [48]. However, as noted in the introduction, there is also interesting physics to be studied for temperatures less than 4 K. Two methods which allow temperature control of the plasma for $T<4$ K are using a dilution refrigerator, or sympathetic cooling by laser-cooled ions [49]. While both these methods are practical, they suffer from being expensive and difficult to implement. However, with advances in space-borne ^{3}He liquefiers, a liquefier well suited for cryogenic ion trap experiments has been developed [50]. These liquefiers act as both refrigerator and thermal isolator allowing the temperature to be varied within the range 0.3 to 30 K. While such a device would not give the lowest achievable temperature, it would give a useful control parameter.

ACKNOWLEDGMENTS

We gratefully acknowledge the support of ONR for this work. We would like to thank Dan Dubin for his help on the mode theory. We would also like to thank Steve Jefferts, Joseph Tan, and Matt Young for their comments on the manuscript.

[1] For reviews see Fred L. Walls and Gordon H. Dunn, Phys. Today **27** (8), 30 (1974); Phys. Scr. **T22**, 21 (1988); Int. J. Mass. Spectrom. Ion Proc. **106**, 1 (1991); J. Mod. Opt. **39**, 193 (1992); Phys. Scr. **46**, 255 (1992); **46**, 544 (1992); Hyperfine Interact. **76**, 3 (1993); D.A. Church, Phys. Rep. **228**, 253 (1993); R. Thompson, Adv. At. Mol. Phys. **31**, 253 (1993).

[2] Daniel H. E. Dubin, Phys. Rev. Lett. **66**, 2076 (1991).

[3] D. J. Heinzen, J. J. Bollinger, F. L. Moore, Wayne M. Itano, and D. J. Wineland, Phys. Rev. Lett. **66**, 2080 (1991).

[4] J. J. Bollinger, D. J. Heinzen, F. L. Moore, W. M. Itano, D. J. Wineland, and D. H. E. Dubin, Phys. Rev. A **48**, 525 (1993).

[5] J. H. Malmberg and J. S. deGrassie, Phys. Rev. Lett. **35**, 577 (1975); A. J. Peurrung and J. Fajans, Rev. Sci. Instrum. **64**, 52 (1993).

[6] Stephan Barlow, Ph.D. thesis, University of Colorado, 1984 (unpublished).

[7] M. D. Tinkle, R. G. Greaves, C. M. Surko, R. L. Spencer, and G. W. Mason, Phys. Rev. Lett. **72**, 352 (1994).

[8] D. J. Wineland, R.E. Drullinger, and F. L. Walls, Phys. Rev. Lett. **40**, 1639 (1978); Wayne M. Itano, L. R. Brewer, D. J. Larson, and D. J. Wineland, Phys. Rev. A **38**, 5698 (1988).

[9] D. L. Eggleston, T. M. O'Neil, and J. H. Malmberg, Phys. Rev. Lett. **53**, 982 (1984).

[10] Robert S. Van Dyck, Jr., Paul B. Schwinberg, and H. G. Dehmelt, in *New Frontiers in High Energy Physics,* edited by Behram Kursunoglu, Arnold Perlmutter, and Linda F. Scott (Plenum, New York, 1978).

[11] Lowell S. Brown and Gerald Gabrielse, Rev. Mod. Phys. **58**, 233 (1986).

[12] G. Gabrielse, S. L. Ralston, L. Haarsma, and W. Kells, Phys. Lett. A **129**, 38 (1988).

[13] Michael E. Glinsky and Thomas M. O'Neil, Phys. Fluids B **3**, 1279 (1991).

[14] A. W. Hyatt, C. F. Driscoll, and J. H. Malmberg, Phys. Rev. Lett. **59**, 2975 (1987).

[15] M. E. Glinsky, T. M. O'Neil, M. N. Rosenbluth, K. Tsurata, and S. Ichimaru, Phys. Fluids B **4**, 1156 (1992).

[16] C. F. Driscoll, J. H. Malmberg, and K. S. Fine, Phys. Rev. Lett. **60**, 1290 (1988).

[17] T. M. O'Neil, Phys.Rev. Lett. **55**, 943 (1985).

[18] D. H. E. Dubin and T. M. O'Neil, Phys. Rev. Lett. **60**, 1286 (1988).

[19] T. M. O'Neil, Phys. Fluids **23**, 2216 (1980).

[20] J. S. deGrassie and J. H. Malmberg, Phys. Fluids **23**, 63 (1980); C. F. Driscoll and J. H. Malmberg, Phys. Rev. Lett. **50**, 167 (1983).

[21] S. A. Prasad and T. M. O'Neil, Phys. Fluids **22**, 278 (1979).

[22] J. B. Jeffries, S. E. Barlow, and G. H. Dunn, Int. J. Mass. Spectrom. Ion Proc. **54**, 169 (1983).

[23] L. R. Brewer, J.D. Prestage, J. J. Bollinger, Wayne M. Itano, D. J. Larson, and D. J. Wineland, Phys. Rev. A **38**, 859 (1988).

[24] J. H. Malmberg and T. M. O'Neil, Phys. Rev. Lett. **39**, 1333 (1977).

[25] S. L. Gilbert, J. J. Bollinger, and D. J. Wineland, Phys. Rev. Lett. **60**, 2022 (1988).

[26] F. Diedrich, E. Peik, J. M. Chen, W. Quint, and H. Walther, Phys. Rev. Lett. **59**, 2931 (1987); D. J. Wineland, J. C. Bergquist, Wayne M. Itano, J. J. Bollinger, and C. H. Manney, *ibid.* **59**, 2935 (1987); Th. Sauter, M. Gilhaus, I. Siemers, R. Blatt, W. Neuhauser, and P. E. Toschek, Z. Phys. D **10**, 153 (1988); G. Birkl, S. Kassner, and H. Walther, Nature **357**, 310 (1992).

[27] C. C. Grimes and G. Adams, Phys. Rev. Lett. **42**, 795 (1979).

[28] Anil Khurana, Phys. Today **14** (12), 17 (1990).

[29] Dr. D. H. E. Dubin has calculated a closed-form solution for the modes in this limit.

[30] Carl S. Weimer, F. L. Moore, and D. J. Wineland, Phys. Rev. Lett. **70**, 2553 (1993).

[31] Earl C. Beaty, J. Appl.Phys. **61**, 2118 (1987).

[32] R. S. Van Dyck, Jr., D. J. Wineland, P. A. Ekstrom, and H. G. Dehmelt, Appl. Phys. Lett. **28**, 446 (1976).

[33] G. Gabrielse, X. Fei, L. A. Orozco, R. L. Tjoelker, J. Haas, H. Kalinowsky, T. A. Trainor, and W. Kells, Phys. Rev. Lett. **65**, 1317 (1990).

[34] H. G. Dehmelt and F. L. Walls, Phys. Rev. Lett. **21**, 127 (1968).

[35] D. Wineland, P. Ekstrom, and H. Dehmelt, Phys. Rev. Lett. **31**, 1279 (1973).

[36] D. J. Wineland and H. G. Dehmelt, J. Appl. Phys. **46**, 919 (1975).

[37] R. S. Van Dyck, Jr., F. L. Moore, D. L. Farnham, P. B. Schwinberg, and H. G. Dehmelt, Phys. Rev. A **36**, 3455 (1987); J. Tan and G. Gabrielse, Phys. Rev. Lett. **67**, 3090 (1991).

[38] F. L. Moore, L. S. Brown, D. L. Franham, S. Jeon, P. B. Schwinberg, and R. S. Van Dyck, Jr., Phys. Rev. A **46**, 2653 (1992).

[39] D. Wineland and H. Dehmelt, Int. J. Mass Spectrom. Ion Phys. **16**, 338 (1975); Erratum **19**, 251 (1976).

[40] D. J. Wineland and W. M. Itano, Phys. Rev. A **20**, 1521 (1979).

[41] D. J. Wineland, J. Appl. Phys. **50**, 2528 (1979); Carl S. Weimer, Ph.D. thesis, Colorado State University, 1992 (unpublished).

[42] John David Crawford and T. M. O'Neil, Phys. Fluids **30**, 2076 (1987).

[43] S. E. Barlow, J. A. Luine, and G. H. Dunn, Int. J. Mass Spectrom. Ion Proc. **74**, 97 (1986).

[44] G. W. Hart, Phys. Fluids B **3**, 2987 (1991); T. B. Mitchell, Ph.D. thesis, University of California at San Diego, 1993 (unpublished).

[45] Claude Cohen-Tannoudji, Metrologia **13**, 161 (1977); Claude Cohen-Tannoudji, Bernard Diu, and Franck Laloe, *Quantum Mechanics I* (Wiley, New York, 1977), pp. 405–411; Eric A. Cornell, Robert Weisskoff, Kevin Boyce, and David E. Pritchard, Phys. Rev. A **41**, 312 (1990).

[46] G. Deville, A. Valdos, E. Y. Andrei, and F. I. B. Williams, Phys. Rev. Lett. **53**, 588 (1984).

[47] D. H. E. Dubin, in *Strongly Coupled Plasma Physics,* edited by H. M. Van Horn and S. Ichimara (University of Rochester Press, Rochester, 1993), pp. 399–406.

[48] G. Savard, St. Becker, G. Bollen, H. J. Kluge, R. B. Moore, Th. Otto, L. Schweikhard, H. Stolzenberg, and U. Wiess, Phys. Lett. A **158**, 247 (1991).

[49] D. J. Larson, J. C. Bergquist, J. J. Bollinger, Wayne M. Itano, and D. J. Wineland, Phys. Rev. Lett. **57**, 70 (1986); D. J. Wineland C. S. Weimer, and J. J. Bollinger, Hyperfine Interac. **76**, 115 (1993).

[50] Franco Pavese and Danilo Ferri, in *Advances in Cryogenic Engineering,* edited by R. W. Fast (Plenum, New York, 1990), Vol. 35.

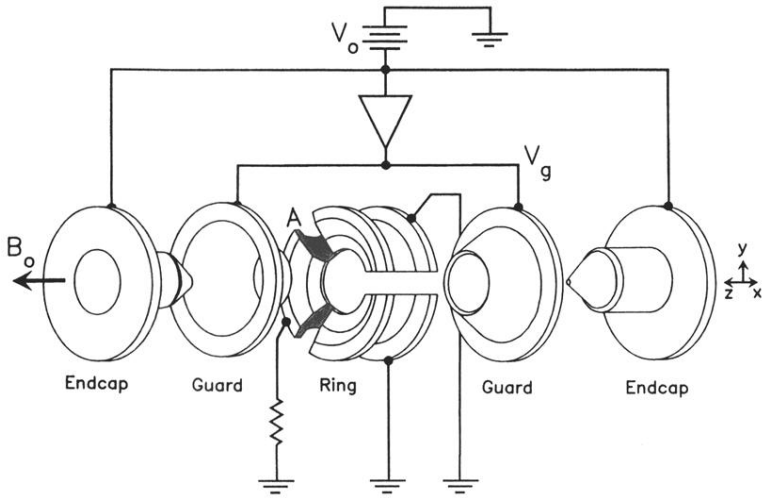

FIG. 1. A schematic diagram of our Penning trap. The electrodes have been separated along the axis to show details. The inner ring diameter is 1 cm.